

## Additives of Suppressing Hydrogen Evolution at Carbon-Containing Negative Plates of Valve-Regulated Lead-Acid Batteries

Jingcheng Hu, Chengbin Wu, Xinle Wang, Yonglang Guo \*

College of Chemistry, Fuzhou University, Fuzhou, 350116, PR China

\*E-mail: [yguo@fzu.edu.cn](mailto:yguo@fzu.edu.cn)

Received: 12 November 2015 / Accepted: 11 December 2015 / Published: 1 January 2016

---

The effects of several rare earth oxides and fluorine-containing compounds as additives on the hydrogen evolution at the negative plates containing commercial and purified carbon materials in valve-regulated lead-acid (VRLA) batteries have been studied by means of the constant current polarization and hydrogen gassing measurements. The activated carbon (AC) and iron impurity in the carbon materials greatly accelerate the hydrogen evolution.  $\text{La}_2\text{O}_3$ ,  $\text{Sm}_2\text{O}_3$ ,  $\text{Gd}_2\text{O}_3$ ,  $\text{Nd}_2\text{O}_3$ ,  $\text{Dy}_2\text{O}_3$  and polytetrafluoroethylene (PTFE) as electrolyte additives inhibit the hydrogen evolution. When the hydrogen evolution polarization potential is small as in the case of the oxygen depolarization in the oxygen cycles, the addition of 0.025% PTFE and 0.025%  $\text{Dy}_2\text{O}_3$  additives to electrolyte increase its overpotential, but these two additives can promote the hydrogen evolution at negative plates containing activated carbon (AC), expanded graphite (EG) or flake graphite (FG) with low impurity contents. In the test of cycle life of the 12 V 12 Ah VRLA batteries with the negative plate containing acetylene black (AB), the combined additive of PTFE and  $\text{Dy}_2\text{O}_3$  greatly increases the charge efficiency and thus decreases water loss.

---

**Keywords:** carbon materials; electrolyte additives; hydrogen evolution; negative plate; valve-regulated lead-acid batteries

### 1. INTRODUCTION

Since the lead-acid battery has many advantages such as low cost, mature technology, high reliability and high efficiency of recycling, it always occupies the largest market in various applications of power sources for a long time. As the valve-regulated lead-acid (VRLA) batteries with absorptive glass mat (AGM) separator or gel electrolyte have increasingly replaced conventional flooded lead-acid batteries, except for 12 V SLI (starting, lighting and ignition) batteries, the demand

for high-power batteries such as uninterruptible power supplies (UPS) and deep-cycle batteries has been increasing significantly [1-2]. In the past decade, much work has been done to investigate the flooded and VRLA batteries in the application of the high-rate partial-state-of-charge (HRPSoC) duty, to reduce CO<sub>2</sub> emission of road transportation vehicles for atmospheric environment [3-7]. These batteries operate in a partial-state-of-charge. And they will be frequently discharged at high power and recharged at an extraordinarily high rate. To meet the requirements and aim of various governments for automakers to decrease CO<sub>2</sub> emission, the micro-hybrid electric vehicles (micro-HEVs) with stop-start and regenerative braking functions will become the main stream [8-10]. Based on different levels of powertrain hybridisation, the lead-acid batteries range from micro- to medium- and full hybrid applications. Lower hybrid degree means higher charge-discharge currents for the batteries. So the VRLA battery fails prematurely due to the progressive build-up of 'hard' lead sulfate on the surface of the negative plates, which markedly reduces the effective surface-area to such extent that the negative plate can no longer deliver and accept the power required by engine cranking, acceleration, and regenerative braking [11].

The Ultrabattery developed by CSIRO Energy Technology combines an asymmetric supercapacitor and a lead-acid battery in one unit cell by connecting internally the carbon-based negative plate (i.e., capacitor electrode) and the lead-acid negative plate in parallel [12-14]. The capacitor electrode acts as a buffer to share the discharge and charge currents at the high rates. Nakamurs [15-16] investigated the performance of the negative plates made with ten times the normal levels of carbon. It indicates that high levels of carbon greatly improve the recharge ability of negative plates by providing conductive networks around the peripheries of lead sulfate crystals and thus extend the battery cycle-life. Since the properties and actions of carbon vary with different morphologies and producing area, a lot of work has been done on what types of carbon can be added to the negative plates in the HRPSoC applications [17-27]. Moseley et al. [19] have summarized that the main function of carbon added to the negative plates is to improve the conductivity, impede the progressive growth of lead sulfate crystals, provide capacitance characteristic buffering high transient current and serve as nuclei of lead sulfate crystal growth as well as an electro-osmotic pump that facilitates acid diffusion. The preferred candidates are the carbons with very high surface area used in supercapacitors and graphite carbon with high surface area. Pavlov [18, 27] proposed the parallel mechanism of PbSO<sub>4</sub> reduction on the electrochemically active carbon (EAC) and Pb surfaces. But the impurities in various carbons can decrease the hydrogen overpotential obviously and water loss becomes the main cause of the subsequent failure mode in the HRPSoC applications [28].

Water loss of VRLA batteries is accompanied by the carbon oxidation, grid corrosion and hydrogen evolution [29-30]. It increases with elevated temperature and high charge-discharge current in the HRPSoC applications. Lam [31] studied the influence of residual elements in lead on hydrogen-gassing and believed that the 'harmful elements' are Ag, As, Co, Cr, Cu, Fe, Mn, Ni, Sb, Se, whereas Bi, Cd, Sn, and Zn have little effect on gassing and are even considered the 'beneficial elements' [32-35]. Oxygen generated at positive plates moves to the surface of negative plates on which it is reduced and makes the negative plate depolarized, which leads to the obvious falling of hydrogen gassing [36-39]. The additives in negative active mass (NAM) have also been widely investigated in order to

suppress hydrogen evolution and sulfation. They include  $\text{Ga}_2\text{O}_3$ ,  $\text{Bi}_2\text{O}_3$ , synthetic lignin, polyaspartate (PASP) and expander components. [40-44].

In this work, the effects of five rare earth oxides and three fluorine-containing compounds as additives on the hydrogen evolution rate at the negative plates containing various carbon materials were studied by means of the measurements of hydrogen polarization curves. A combined electrolyte additive was added to the 12 V 12 Ah VRLA battery. Water loss and charge efficiency were explored.

## 2. EXPERIMENTAL

### 2.1. Preparation of test negative plate

The paste of the test negative plate was prepared by mixing leady oxide,  $\text{H}_2\text{SO}_4$ ,  $\text{H}_2\text{O}$  and additives which were composed of commercial barium sulfate, sodium lignosulfonate (Vanisperse A), fiber and different carbon materials. The carbon materials used were carbon black (CB), activated carbon (AC), acetylene black (AB), flake graphite (FG) and expanded graphite (EG). The paste contained 40 g  $\text{H}_2\text{SO}_4$  per 1 kg lead powder and its apparent density was 4.1-4.3 g  $\text{cm}^{-3}$  based on different carbon materials. 18.5 g paste was pasted by hand on Pb-Ca-Al grid with the dimensions of 44.3 (W)×73 (H)×1.5 (T) mm. And the negative plate was cured and dried in a high and low temperature-humidity test chamber (GD/HS4010, Shanghai) for two days. Then the plate was formed in 1.05 sp gr  $\text{H}_2\text{SO}_4$  solution at constant current of 500 mA for 14 h + 200 mA for 12.5 h. After that the formed plate was washed by 1.28 sp gr  $\text{H}_2\text{SO}_4$  solution and then was soaked in bulk solution with 1.28 sp gr  $\text{H}_2\text{SO}_4$  for 24 h to avoid the oxidation of fresh sponge lead on the negative plate and to ensure the consistency of  $\text{H}_2\text{SO}_4$  concentration in the next experiments.

The purification of the carbon materials was carried out according to the following treatment: 10 g carbon was added to about 200 ml 1.28 sp gr  $\text{H}_2\text{SO}_4$  solution. Stir the suspension for 4 h, wash the

**Table 1.** Metal impurity contents in different carbon materials

Carbons in negative plates	Negative plate numbers	Carbon contents	Metal impurity contents / ppm					
			Fe	Cu	Sb	Mn	Co	Ni
No carbon (NC)	NC	-	-	-	-	-	-	-
Acetylene black (AB)	AB#1	0.5%	10	★	★	★	★	★
	AC#1	0.5%	870	★	★	★	★	★
Activated carbon (AC)	AC#2	0.5%	56	★	★	★	★	15
	Carbon black (CB)	CB#1	0.2%	★	16	★	88	★
Expanded graphite (EG)	EG#1	1.5%	2370	56	★	53	★	23
	EG#2	1.5%	340	29	★	★	★	★
	EG#3	1.5%	21	★	★	28	★	★
Flake graphite (FG)	FG#1	2%	1640	★	★	12	★	★
	FG#2	2%	25	★	★	★	★	★

Notes: #1 denotes the commercial carbon materials; #2 and #3 the purified carbon materials.

- : none; ★: metal impurity content <10 ppm.

carbon material by means of dilute  $\text{H}_2\text{SO}_4$  solution and filter out impurities. Then the as-prepared carbon was dispersed into the  $\text{H}_2\text{SO}_4$  solution again, filtrated, washed with double-distill water and then dried in a vacuum oven at  $80\text{ }^\circ\text{C}$  for 4 h. The impurity contents of the commercial and purified carbon materials were listed in Table 1.

## 2.2. Measurement of hydrogen evolution

The formed negative plate as working electrode was put into a bag made by the polyethylene (PE) separator. Two positive plates as counter electrode were placed at both sides of the working electrode and the  $\text{Hg}/\text{Hg}_2\text{SO}_4/1.28\text{ sp gr H}_2\text{SO}_4$  electrode was used as reference electrode. The three-electrode electrolytic cell was in a water bath at  $25\pm 0.2\text{ }^\circ\text{C}$ , as shown in Fig. 1. In the measurement process, the hydrogen generated at working electrode in the cathodic polarization does not pass through the PE bag but escape from the liquid surface in the bag and the oxygen gassing from positive plate outside the PE bag does not reach the negative plate either. So only hydrogen is collected by a cap connecting a foam flowmeter (Fig. 1) which is used to measure the volume of hydrogen gassing.

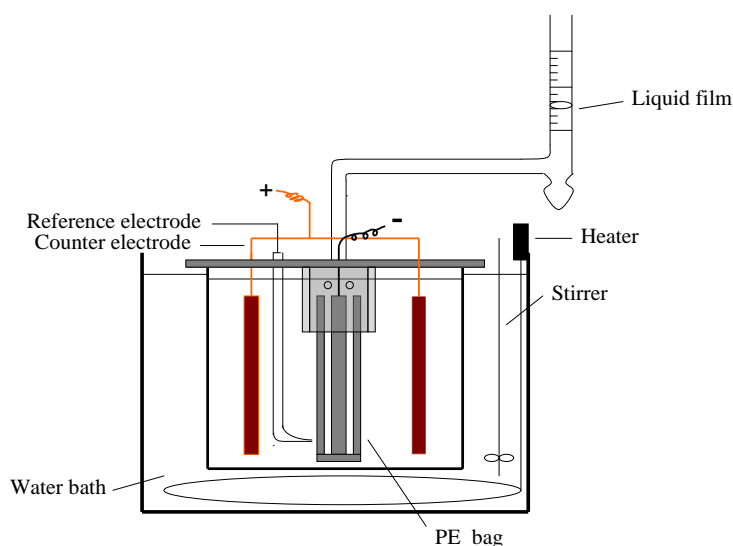


**Figure 1.** Apparatus used to determine hydrogen gassing.

The formed negative plate was taken out of the soaked solution with  $1.28\text{ sp gr H}_2\text{SO}_4$  and moved into the electrolyte cell containing  $1.28\text{ sp gr H}_2\text{SO}_4$  solution immediately. Then it was polarized cathodically at  $10\text{ mA}$  for  $16\text{ h}$  to make the negative active mass transformed into sponge lead completely and de-aerate the  $\text{H}_2\text{SO}_4$  electrolyte in the bag. Finally, the cathodic polarization was carried out at constant current of  $8\text{ mA}$  for  $2\text{ h}$ , in which the volume of hydrogen gassing was measured when the polarization potential was stable. The currents of cathodic polarization were changed in turn from  $8, 7, 6, 5, 3$  to  $2\text{ mA}$ . The experiments were conducted at the room temperature of  $25\pm 1\text{ }^\circ\text{C}$ .

### 2.3. Additives

All rare earth oxide reagents with analytical grade (AR) and commercial perfluorinated compounds were used as received without any further treatment. The rare earth additives of  $\text{La}_2\text{O}_3$ ,  $\text{Sm}_2\text{O}_3$ ,  $\text{Gd}_2\text{O}_3$ ,  $\text{Nd}_2\text{O}_3$  and  $\text{Dy}_2\text{O}_3$  with different contents were directly added to the 1.28 *sp gr*  $\text{H}_2\text{SO}_4$  electrolyte due to their dissolubility. Since the solubility of the pentadecafluorooctanoic acid (PFOA) and perfluorooctanesulfonic acid potassium (PFOSAP) is very poor, these fluorine-containing additives were dispersed into  $\text{H}_2\text{SO}_4$  solution via the ultrasound treatment and then added to the paste in the preparation of the negative plates. The polytetrafluoroethylene (PTFE) was used as additives in both the  $\text{H}_2\text{SO}_4$  electrolyte and the paste of negative plate, but it needs to be pretreated by the ultrasonic dispersion before use.

### 2.4. Test batteries

The test batteries were the 6-DZM-12 VRLA batteries (12 V 12 Ah) used for electric bike, produced by Chaowei Power Co. Ltd., China. The 1.255 *sp gr*  $\text{H}_2\text{SO}_4$  solution with the combined electrolyte additives of 0.025% PTFE + 0.025%  $\text{Dy}_2\text{O}_3$  was pretreated ultrasonically and then used for the container formation. The cycle life test was conducted by Land battery test instrument (CT2001B) according to the operating conditions of the electric bike batteries, namely, the batteries were discharged at  $C_2$  rate to 10.5 V with 100% depth of discharge (DOD) and then were charged to 14.75 V at 2.5 A. When the charge current at 14.75 V dropped to 0.35 A, they were charged at this voltage for 4 h again. The battery capacity and charge efficiency were measured and the batteries were weighed to calculate the water loss in the cycle-life test.

### 2.5. Impurity measurement and characterization

The measurement for the impurities of the purified carbon was carried out by the inductively coupled plasma atomic emission spectrometry (Thermo iCAP 6000). The appearances of the carbon materials were observed by the scanning electron microscope (SEM, Zeiss, Supra 55). The apparent density, specific area and mean particle size of carbon materials were measured by the accelerated surface area and porosimetry system (ASAP 2020M).

## 3. RESULTS AND DISCUSSION

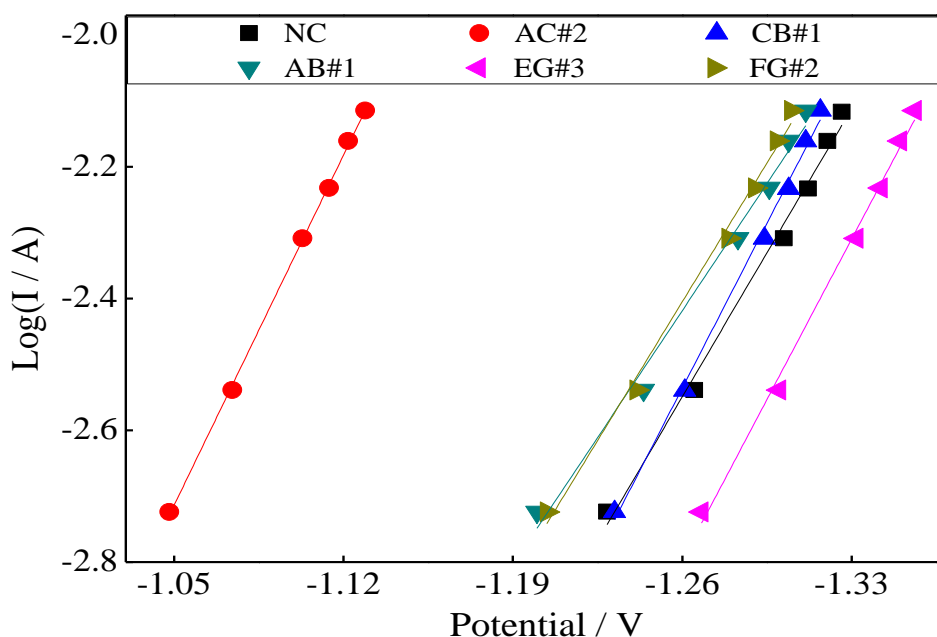
### 3.1. Effects of additives

The oxygen generated at positive plate in the VRLA batteries moves to the negative plate at which it can be reduced easily, but it is very difficult for the hydrogen produced at negative plate to be oxidized at the positive plate because of slow kinetics, which leads to water loss. In the oxygen cycle in VRLA batteries, the negative plate can be depolarized obviously. So the negative plate almost works

near the Pb/PbSO<sub>4</sub> equilibrium potential, though it is overcharged. It means that the current of hydrogen evolution is normally very small at negative plates. So the selected current range is only from 2 to 8 mA in the experiments of hydrogen gassing. In order to accurately measure the hydrogen evolution rate, it is important to control the electrolyte temperature, to ensure the full charge for the negative plate and to precisely measure the volume of hydrogen gassing. In Fig. 1, a bubble of detergent was squeezed into the burette when the potential of the negative plate was stable. The hydrogen evolution volume, *V*, was measured after a period, *t*. The hydrogen evolution current, *I*<sub>H<sub>2</sub></sub>, can be calculated by the following relationship [31]

$$I_{H_2} = \frac{2FV(P_{total} - P_w)}{10^6 RTt} \tag{1}$$

where *P*<sub>total</sub> denotes atmospheric pressure (101,325 Pa); *P*<sub>w</sub> vapour pressure (3167 Pa); *T* absolute temperature (298 K); *F*=96500 C mol<sup>-1</sup>; *R*=8.31 J mol<sup>-1</sup> K<sup>-1</sup>;



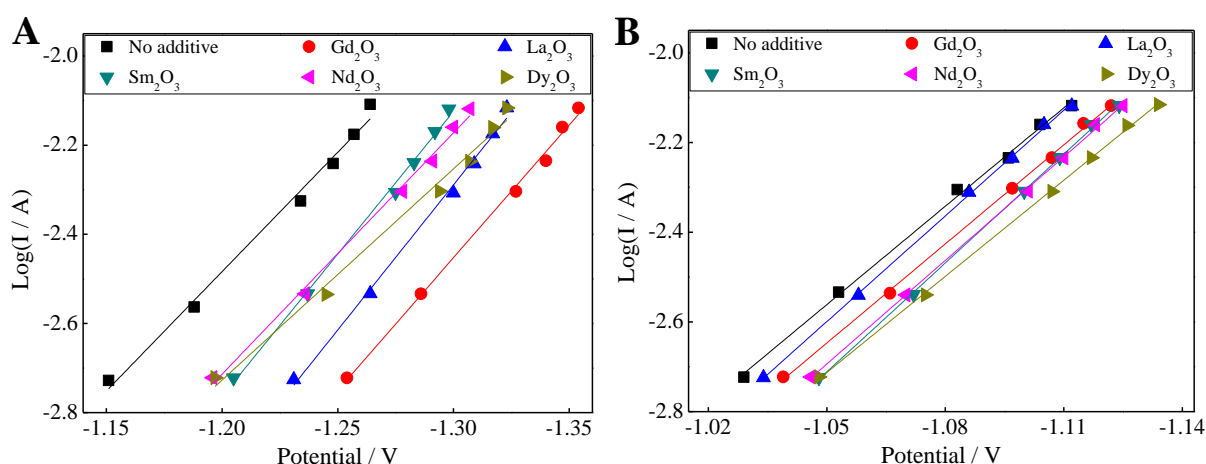
**Figure 2.** Polarization curves of hydrogen evolution at negative plates containing different carbons with low impurity contents in 1.28 sp gr H<sub>2</sub>SO<sub>4</sub> solution.

Fig. 2 shows the polarization curves of hydrogen evolution at negative plates containing different types of carbon with low impurity contents (Table 1). Although the impurity contents of all carbon materials after purification are very low, in comparison with the NC sample without carbon, the AC#2 negative plate containing activated carbon makes the polarization potential of hydrogen evolution on average decrease by 194 mV, which may be closely related to its porous structure with very high specific area shown in Table 2. Both AB#1 and FG#2 negative plates decrease by about 20 mV but the EG#3 negative plate increases by 33 mV. No obvious effect on the CB#1 sample electrode is detected.

**Table 2.** Properties of carbon materials

Carbons	Apparent density / g m <sup>-3</sup>	Specific area / m <sup>2</sup> g <sup>-1</sup>	Mean particle size / nm
Acetylene black (AB)	0.038	63.8	94.1
Activated carbon (AC)	0.223	1005.0	6.0
Carbon black (CB)	0.047	450.2	14.4
Expanded graphite (EG)	0.226	601.5	1.77×10 <sup>4</sup>
Flake graphite (FG)	0.181	8.3	1.95×10 <sup>4</sup>

Carbon black (CB) is widely used as an additive in the negative plates of flood and VRLA batteries [18-20, 22]. To inhibit the passivation of PbSO<sub>4</sub> on the surface of the negative plate in the HRPSoC application of lead-acid batteries, a large amount of activated carbon (AC) as additive is added to the paste of the negative plate[24, 26-28], which accelerates the hydrogen evolution. Considering the maximum amount of activated carbon for the paste operability, Fig. 3 shows the changes of the cathodic polarization potential of hydrogen evolution at the negative plates containing 0.2% commercial carbon black (CB#1) and 0.5% commercial activated carbon (AC#1), and the effects of rare earth oxides as the electrolyte additives. It is clear from Fig. 3A and 3B that the polarization potential of hydrogen evolution at the negative plate containing 0.5% activated carbon in the H<sub>2</sub>SO<sub>4</sub> solution without rare earth oxide additives decreases by about 120 mV, compared with the negative plate containing 0.2% carbon black.



**Figure 3.** Polarization curves of hydrogen evolution at negative plates containing (A) 0.2% carbon black (CB#1) and (B) 0.5% activated carbon (AC#1) in 1.28 sp gr H<sub>2</sub>SO<sub>4</sub> solution containing different rare earth oxides. Additive concentration: 0.025%.

Lam [31] studied the maximum acceptable levels (MALs) in raw lead materials beyond which the residual elements or impurities in other materials will lead to obvious hydrogen evolution. The

upper level of Fe, Sb, Ni, Cu and Co is lower than 10 ppm and that of Mn is lower than 3 ppm. It is clear from Table 1 that the increase of hydrogen evolution is mainly due to the fact that the commercial activated carbon (AC#1) contains a lot of iron impurity which depends on its production processes. Another reason is that the activated carbon (AC) has porous structure with very high specific area. The five additives of rare earth oxides increase the polarization potentials of hydrogen evolution at both negative plates to a certain extent. In Fig. 3A, their effect order is  $Gd_2O_3 > La_2O_3 > Dy_2O_3 > Nd_2O_3 \sim Sm_2O_3$  at the negative plate containing 0.2% carbon black and in Fig. 2B, it is  $Dy_2O_3 > Nd_2O_3 \sim Sm_2O_3 > Gd_2O_3 > La_2O_3$  at the negative plate containing 0.5% activated carbon. This is because these rare earth oxides are soluble and rare earth metal ions with high valence may adsorb at the surface of negative active mass, which will prohibit the hydrogen ions from coming closer to the electrode surface.

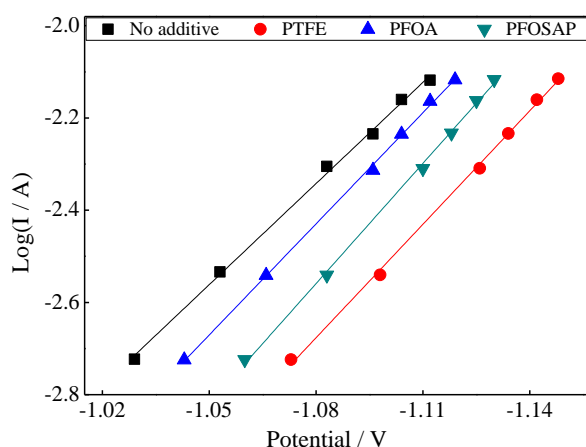


**Figure 4.** Polarization curves of hydrogen evolution at negative plates containing 0.5% activated carbon (AC#1) in 1.28 *sp gr*  $H_2SO_4$  solution. PTFE, PFOA and PFOSAP were added into the paste of negative plates. Additive amount: 0.05%.

Activated carbon (AC) is often added to the negative plate in the HRPSoC application of lead-acid batteries, but it can result in the increase of hydrogen evolution [22, 26-28]. Since only fluorine-containing organic compounds can be stable in the lead-acid battery system, three fluorine-containing compounds as additives were added to the paste of the negative plates due to their limited dissolubility in  $H_2SO_4$  solution. Fig. 4 shows the cathodic polarization curves of hydrogen evolution at the negative plates containing 0.5% commercial activated carbon (AC#1). The effect order is PTFE > PFOSAP > PFOA and the PTFE additive increases the cathodic polarization potential by about 40 mV. The effects of these fluorine-containing organic compounds may be due to their adsorption at the surface of the negative electrode.

Fig. 5 shows the polarization curves of hydrogen evolution at the negative plate without carbon and the effects of PTFE as an electrolyte additive. In comparison with the negative plate without carbon in Fig. 5, the addition of 0.2% carbon black (CB#1) and 0.5% activated carbon (AC#1) to the negative pastes in Fig. 3 causes the polarization potentials to drop by 80 and 200 mV, respectively.



This is due to the increase of the specific area and the impurity effects when the commercial carbons are added. However, it can be seen from Fig. 5 that the PTFE electrolyte additive increases the hydrogen evolution potential by about 90 mV at the negative plates without carbon.

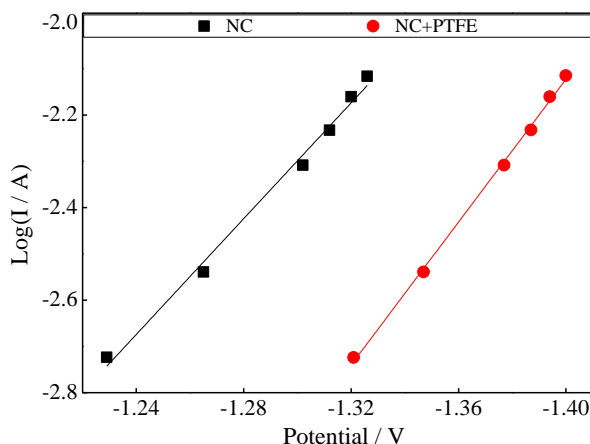


**Figure 5.** Polarization curves of hydrogen evolution at negative plates without carbon in 1.28 *sp gr* H<sub>2</sub>SO<sub>4</sub> solution with and without 0.025% PTFE additive.

### 3.2. Effects of additive concentrations

Considering the nonuniformity of fluorine-containing compounds in the paste and their stability in the electrolyte of lead-acid batteries, the effects of fluorine-containing compounds as electrolyte additives on hydrogen evolution were investigated.

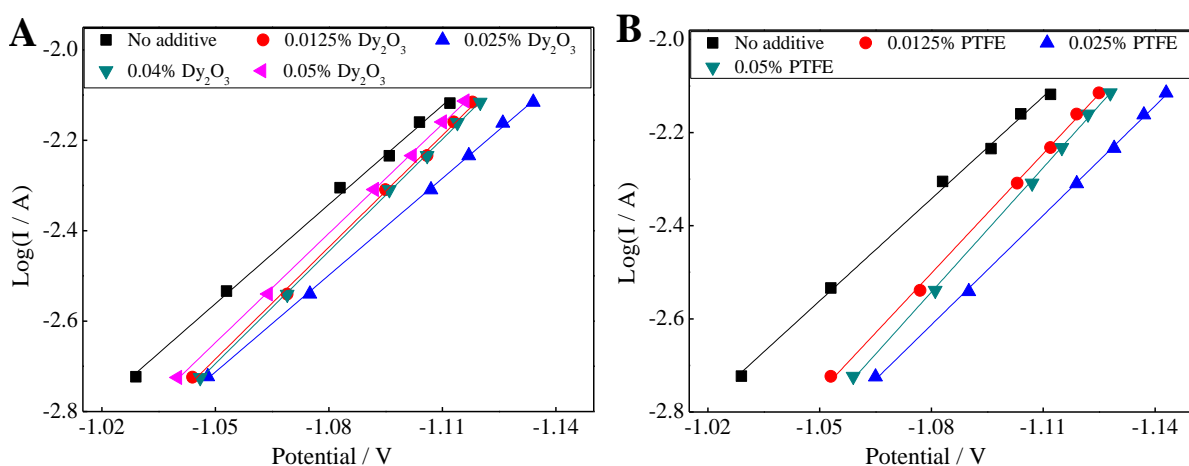


**Figure 6.** Polarization curves of hydrogen evolution at negative plates with 0.5% activated carbon (AC#1) in 1.28 *sp gr* H<sub>2</sub>SO<sub>4</sub> solutions containing different concentrations of (A) Dy<sub>2</sub>O<sub>3</sub> and (B) PTFE.

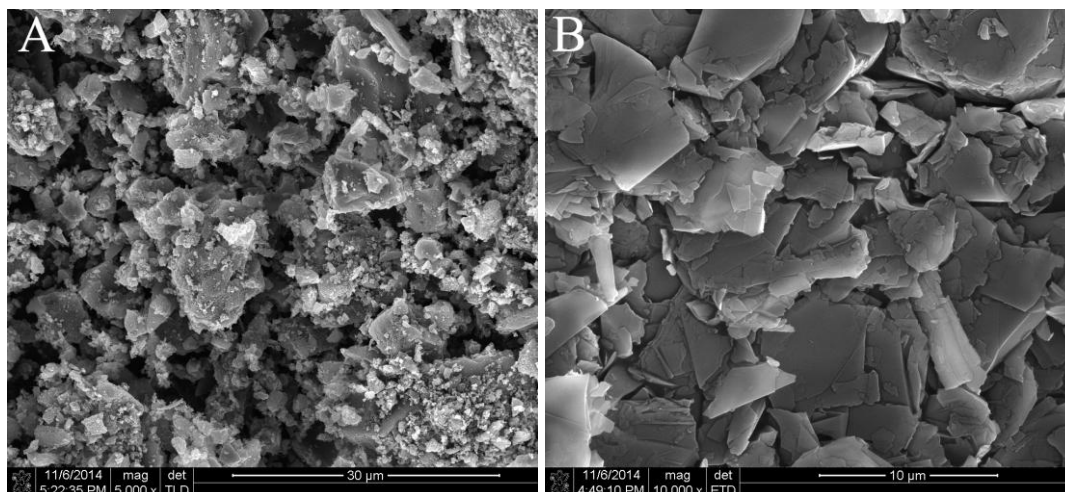
Although Fig. 3A indicates that the additives of both Gd<sub>2</sub>O<sub>3</sub> and La<sub>2</sub>O<sub>3</sub> have more negative polarization potential of hydrogen evolution at the negative plates containing 0.2% carbon black,

activated carbon in Fig. 3B has porous structure with very high specific surface area and its capacitance characteristic is superior to that of other types of carbon. The negative plates used in the HRPSoC application of lead-acid batteries are expected to contain activated carbon and have the capacitance characteristics with high performance in the charge-discharge at very high rate.

However, the iron impurity in commercial active carbon can promote the hydrogen evolution. How to suppress hydrogen evolution at the negative plates containing active carbon has drawn much attention. Based on the results in Fig. 3B and Fig. 4, the electrolyte additives of  $\text{Dy}_2\text{O}_3$  and PTFE were studied next. Fig. 6 shows the effects of different concentrations of  $\text{Dy}_2\text{O}_3$  and PTFE in the electrolytes on hydrogen evolution rate at negative plates with 0.5% activated carbon (AC#1). Both additives with different concentrations increase the polarization potentials of hydrogen evolution. And the effect order of  $\text{Dy}_2\text{O}_3$  additive is  $0.025\%\text{Dy}_2\text{O}_3 > 0.04\%\text{Dy}_2\text{O}_3 \sim 0.0125\%\text{Dy}_2\text{O}_3 > 0.05\%\text{Dy}_2\text{O}_3$  and for PTFE additive, it is  $0.025\%\text{PTFE} > 0.05\%\text{PTFE} > 0.0125\%\text{PTFE}$ . Therefore, both additives with 0.025% content in the electrolyte have the most negative cathodic polarization potentials at negative plates containing 0.5% activated carbon and they will be investigated in the following sections.

### 3.3. Effects of carbon materials and impurities

Table 1 shows the main metal impurity contents in five commercial carbon materials (#1) and those after the purification treatments (#2 and #3). Carbon black (CB) and acetylene black (AB) are the common additives in lead-acid batteries and can be used as received because of very low impurity contents. In comparison with the acceptable upper level proposed in ref [31], however, the other three kinds of commercial carbon materials (#1) have very high iron content which depends on their producing area and production processes. It indicates from Table1 that the impurities in the commercial activated carbon and commercial graphites are mainly iron and the contents of other impurities are relatively low. Table 2 shows the apparent density, specific area and mean particle size of different carbon materials.



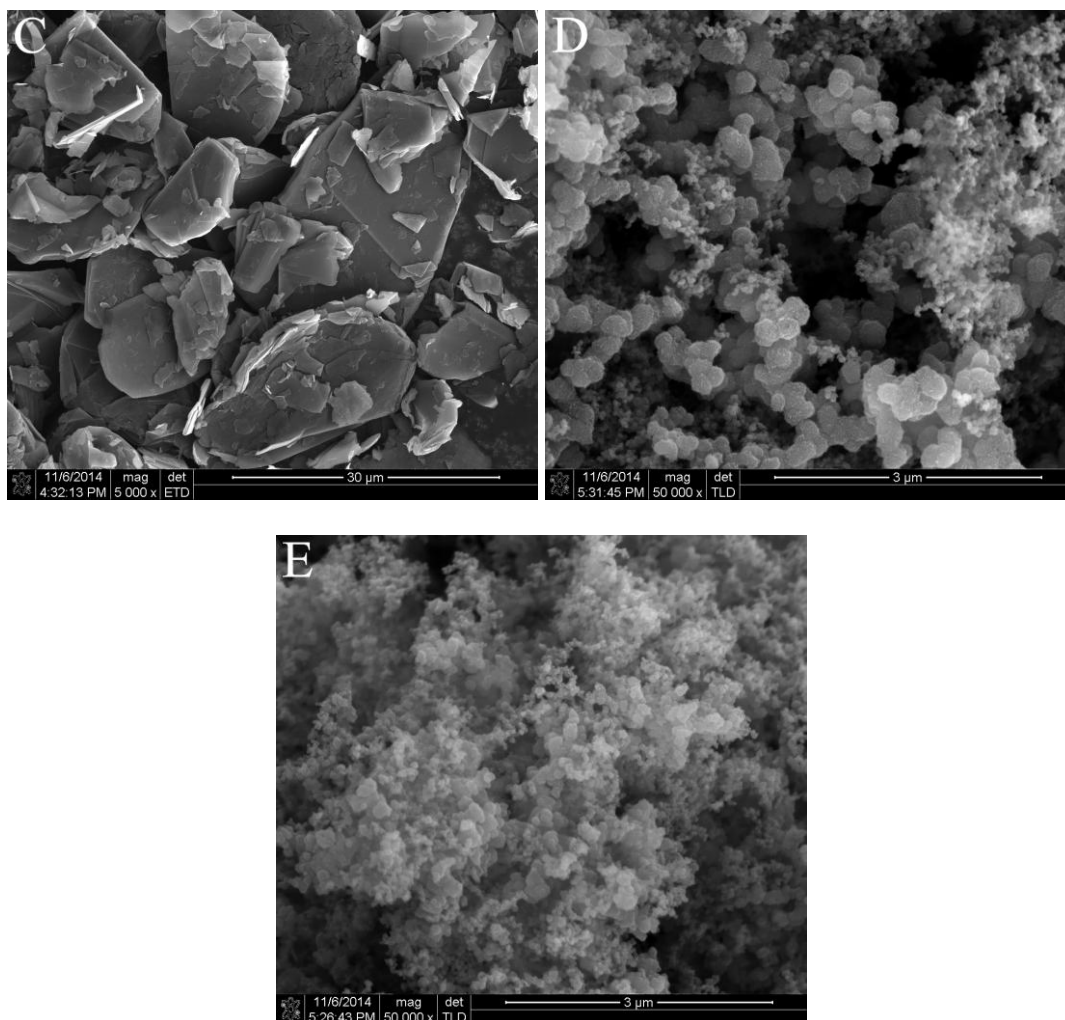


**Figure 7.** SEM images of different carbon materials. (A) activated carbon, (B) expanded graphite, (C) flake graphite, (D) carbon black, (E) acetylene black.

It indicates that the activated carbon (AC) has the highest specific area and the smallest mean particle size, which can increase the surface area of negative active mass and decrease the current density and polarization of hydrogen evolution. The order of the specific area is  $AC > EG > CB > AB > FG$ , but the order of mean particle size is  $FG > EG > AB > CB > AC$ . Both EG and FG have very large mean particle sizes. And AB and CB have the smallest apparent density.

Fig. 7 shows the SEM images of the five commercial carbon materials. The order of particle size is  $FG > EG > AC > CB > AB$ .

Activated carbon (AC) in Fig. 7A presents more pores in its aggregation. Expanded graphite (EG) with very thin flake-structure in Fig. 7B accumulates together and their fragments milled in the production are clearly visible. Flake graphite (FG) in Fig. 7C has biggest particle size. Carbon black (CB) in Fig. 7D shows the circular structure and acetylene black (AB) in Fig. 7E has very small particles but obvious aggregation. Their difference between the data in Table 2 and SEM images in Fig. 7 depends on the aggregation and their structures.

Activated carbon with very large specific area has the property of supercapacitor and is often added to the negative plate to inhibit the passivation of lead sulfate in the HRPSOC application of lead-acid batteries [22,26-27]. But activated carbon can accelerate the hydrogen evolution greatly [28]. Fig. 8 shows the polarization curves of hydrogen evolution at negative plates containing activated carbon in the H<sub>2</sub>SO<sub>4</sub> solution both without and with electrolyte additives. For the negative plate containing AC#1 in which there is a lot of iron impurity, the addition of PTFE, Dy<sub>2</sub>O<sub>3</sub> and Dy<sub>2</sub>O<sub>3</sub> + PTFE on average increases the polarization potential of hydrogen evolution by 34, 21 and 19 mV, respectively.

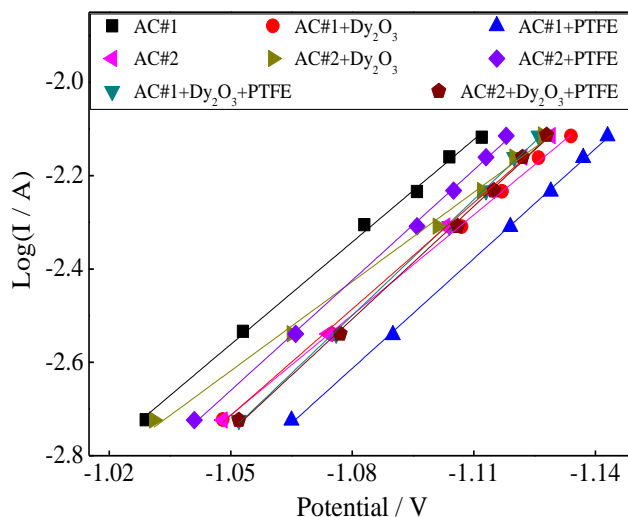


**Figure 8.** Polarization curves of hydrogen evolution at negative plates with 0.5% activated carbon in 1.28 *sp gr* H<sub>2</sub>SO<sub>4</sub> solution without and with electrolyte additives of 0.025%PTFE, 0.025% Dy<sub>2</sub>O<sub>3</sub> and 0.025% Dy<sub>2</sub>O<sub>3</sub> + 0.025%PTFE.

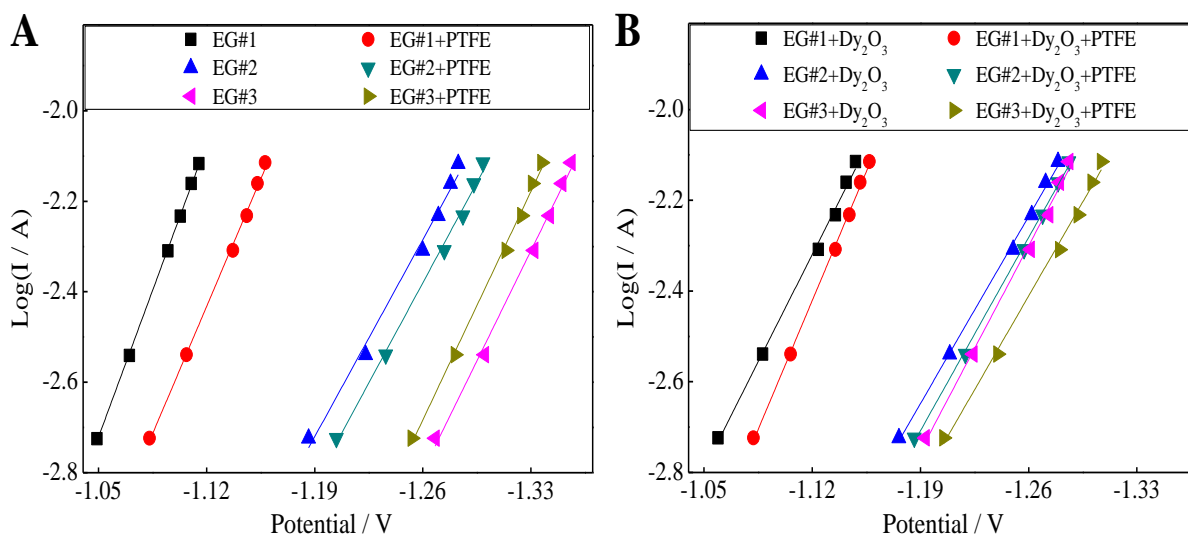


**Figure 9.** Polarization curves of hydrogen evolution at negative plates with 1.5% expanded graphite containing different impurity contents in 1.28 *sp gr* H<sub>2</sub>SO<sub>4</sub> solution without and with electrolyte additives of 0.025%PTFE, 0.025% Dy<sub>2</sub>O<sub>3</sub> and 0.025% Dy<sub>2</sub>O<sub>3</sub> + 0.025%PTFE.

After the commercial activated carbon (#1) was purified, the three kinds of electrolyte additives mentioned above do not affect the hydrogen evolution of the negative plate containing purified activated carbon (AC#2) much. In the presence of PTFE, the AC#1 sample with high iron content has lower hydrogen evolution rate in comparison with AC#2 with low iron content. This is because the AC#1 and AC#2 samples have very small hydrogen evolution overpotential and the standard electrode potential of  $\text{Fe}^{2+}/\text{Fe}$  (-0.447 V) is only 91 mV negative to that of  $\text{PbSO}_4/\text{Pb}$  (-0.356 V). At this time, the  $\text{Fe}^{3+}$  ions is reduced to  $\text{Fe}^{2+}$  ions rather than Fe at the surface of the electrode and the presence of  $\text{Fe}^{2+}$  ions can inhibit the  $\text{H}^+$  ions to access the surface of electrode, which slows down hydrogen evolution.

EG#1 is the negative plate prepared by the commercial expanded graphite with very high iron content and some copper impurity. EG#2 and EG#3 are those made by the purified EGs with different impurity contents. Fig. 9 shows the effects of three kinds of expanded graphite with different impurity contents on the hydrogen evolution at the negative plates. In Fig. 9A, the polarization potentials of the hydrogen evolution at EG#2 and EG#3 negative plates increase by 170 and 234 mV with the decrease of the iron contents from 2370 to 340 and 21 ppm corresponding to EG#1, EG#2 and EG#3 negative plates, respectively. The PTFE additive in the electrolyte causes the polarization potentials of hydrogen evolution at EG#1 and EG#2 negative plates to increase by 40 and 15 mV, but EG#3 negative plate decreases by 18 mV reversely. For EG#1 negative plate containing high impurity content in Fig. 9B, the electrolyte additives of  $\text{Dy}_2\text{O}_3$  and  $\text{Dy}_2\text{O}_3 + \text{PTFE}$  on average increase the polarization potentials of hydrogen evolution by 26 and 39 mV, respectively, compared with EG#1 negative plate in the solution without the electrolyte additive in Fig. 9A. But, they decrease reversely by 72 and 54 mV at EG#3 negative plate. And they do not affect EG#2 negative plate much. This is because the iron and copper impurities are reduced to metal Fe and Cu at the polarization potential in Fig. 9.

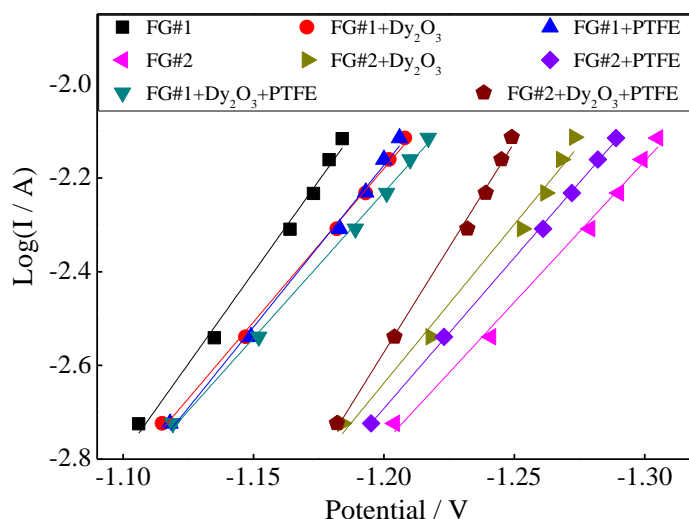


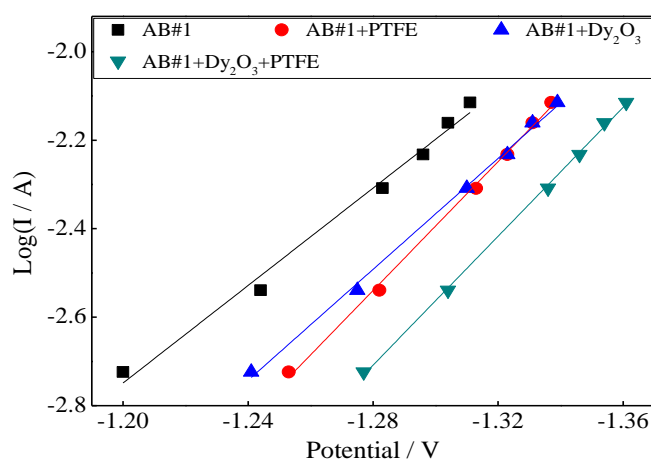
**Figure 10.** Polarization curves of hydrogen evolution at negative plates containing 2% flake graphite in 1.28 *sp gr*  $\text{H}_2\text{SO}_4$  solution without and with electrolyte additives of 0.025% PTFE, 0.025%  $\text{Dy}_2\text{O}_3$  and 0.025%  $\text{Dy}_2\text{O}_3 + 0.025\%$  PTFE.

Hydrogen can generate from metal Fe, Cu, expanded graphite or negative active mass containing other additives, and the order of its evolution overpotential is negative active mass > expanded graphite > Fe > Cu. Therefore, the three electrolyte additives inhibit the hydrogen evolution at the negative plates with high iron content or low hydrogen overpotential while they can accelerate the hydrogen evolution when the impurity content is very low and the hydrogen evolution overpotential is very high.

Fig. 10 shows the polarization curves of hydrogen evolution at negative plates containing flake graphite (FG). The effects of the three additives on the hydrogen evolution rate mainly depend on the impurity contents in flake graphite. The hydrogen evolution overpotential at FG#2 negative plate containing low iron content increases obviously compared with FG#1 negative plate containing high iron content. However, the effects of the three additives on the two negative plates with different impurity contents are just opposite. For FG#1 negative plate with high iron content and low hydrogen overpotential, the three additives increase the hydrogen evolution overpotential, while they decrease the hydrogen evolution overpotential when the iron content is very low and the overpotential of hydrogen evolution is high at FG#2 negative plate. It is similar to the expanded graphite. When the hydrogen evolution polarization potential shifts in the negative direction, the iron impurity is reduced to metal Fe, which decreases hydrogen evolution overpotential greatly.

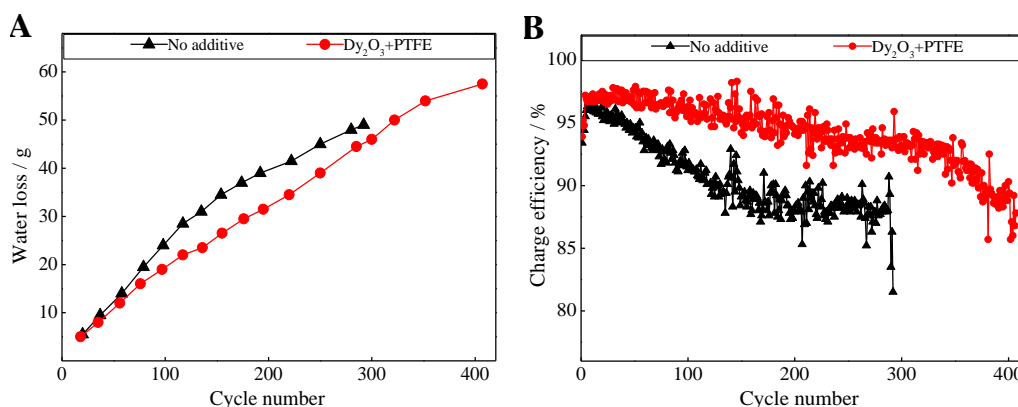
### 3.4. Effects of additives on battery cycle life

Fig. 11 shows the effects of the electrolyte additives on the hydrogen evolution rate at the negative plate containing acetylene black. The order of additive effect is  $\text{Dy}_2\text{O}_3 + \text{PTFE} > \text{PTFE} \sim \text{Dy}_2\text{O}_3 > \text{no additive}$ . Both  $\text{Dy}_2\text{O}_3$  and PTFE additives make the polarization potential of hydrogen evolution increase by 30-34 mV and the combined additive of  $\text{Dy}_2\text{O}_3$  and PTFE makes it increase by 57 mV.



**Figure 11.** Polarization curves of hydrogen evolution at negative plates containing 0.5% acetylene black in 1.28 *sp gr*  $\text{H}_2\text{SO}_4$  solution without and with electrolyte additives of 0.025% PTFE, 0.025%  $\text{Dy}_2\text{O}_3$  and 0.025%  $\text{Dy}_2\text{O}_3 + 0.025\%$  PTFE.

Acetylene black or carbon black was widely used as an additive at the negative active mass in the VRLA batteries. Based on the results in Fig. 11, a combined electrolyte additive of  $\text{Dy}_2\text{O}_3 + \text{PTFE}$  was added to the 12 V 12 Ah VRLA battery with the negative plate containing acetylene black when the battery was formed. Fig. 12 shows the effects of the combined additive on water loss and charge efficiency in the test of the battery cycle life. It can be seen from Fig. 12A that the combined additive greatly reduces the water loss of the test battery from the 60<sup>th</sup> to 120<sup>th</sup> cycles compared with the contrast battery without additive. After that, the water loss rate of both batteries is similar and then that of the contrast battery becomes a little slow. Fig. 12B indicates that the combined additive obviously improves the charge efficiency of the test battery. The charge efficiency of the contrast battery drops linearly before the 120<sup>th</sup> cycle and then becomes slow. The lower charge efficiency means the higher oxygen cycle current. As a result, the potentials of positive and negative plates shift in the positive direction at a constant charge voltage. Therefore, the low hydrogen evolution rate leads to reduction of water loss rate of the contrast battery after the 180<sup>th</sup> cycle in Fig. 12A.



**Figure 12.** The changes of (A) water loss and (B) charge efficiency in the cycles of 12 V 12Ah VRLA batteries without and with the combined electrolyte additive of 0.025%  $\text{Dy}_2\text{O}_3 + 0.025\%$  PTFE.

Fig. 13A shows the changes of the 100% DOD capacity of the test and contrast batteries. The increase of the battery capacity near the 146<sup>th</sup> cycle is due to the rising of the environmental temperature caused by the laboratory air-condition failure in the summer. The capacity of the test battery with the combined electrolyte additive drops slowly and still keeps 87.7% rated capacity in the 400<sup>th</sup> cycle. However, the capacity of the contrast battery without additive begins to fall quickly after 260 cycles and is lower than 80% nominal capacity in the 290<sup>th</sup> cycle.

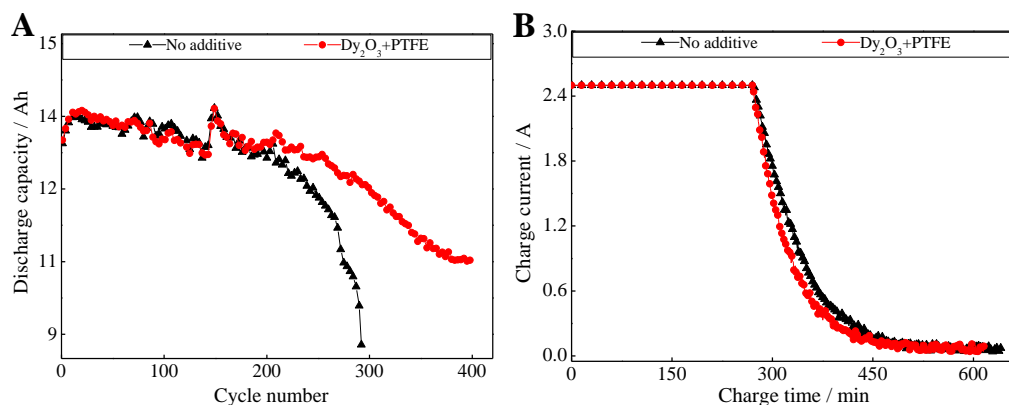


**Figure 13.** The changes of (A) discharge capacity in the cycles and (B) charge current in the 200<sup>th</sup> cycle for 12 V 12Ah VRLA batteries without and with combined electrolyte additive of 0.025% Dy<sub>2</sub>O<sub>3</sub> + 0.025% PTFE.

The teardown analysis shows that the failure battery is caused by the serious corrosion of the positive grids. Fig. 13B shows the change of the charge current of both batteries. At the stage of the limited or constant voltage, the battery without additive has the higher charge current. It means the oxygen cycle current of the contrast battery is larger and the test battery with additive has higher charge efficiency which is in agreement with the results in Fig. 12B. The higher oxygen cycle current leads to the higher positive polarization potential, which is one of the reasons for the positive grid corrosion.

#### 4. CONCLUSIONS

In the HRPSoC application of lead-acid batteries, various carbon materials are added to the negative plate, which affects the hydrogen evolution rate greatly and this depends on the material morphologies and the impurity content. The negative plate without carbon has very high cathodic polarization potential of hydrogen evolution. When the impurity content is very low, the addition of 0.2% carbon black (CB), 0.5% acetylene black (AB), 2% flake graphite (FG) or 1.5% expanded graphite (EG) to the negative plates only affects 20-30 mV overpotential for the hydrogen evolution. But 0.5% activated carbon (AC) in the negative active mass makes its polarization potential decrease by about 194 mV because activated carbon has very high specific area.

Five electrolyte additives of La<sub>2</sub>O<sub>3</sub>, Sm<sub>2</sub>O<sub>3</sub>, Gd<sub>2</sub>O<sub>3</sub>, Nd<sub>2</sub>O<sub>3</sub> and Dy<sub>2</sub>O<sub>3</sub> rare earth oxides inhibit the hydrogen evolution at the negative plates containing 0.2% CB or 0.5% AC. The fluorine-containing additives of PTFE, PFOA and PFOSAP also increase polarization potential of hydrogen evolution. The function of various additives for the negative plates containing different carbons is different. And the effects of the activated carbon and the impurities in various commercial carbon materials are dominant. When iron content in carbon materials is very high and the hydrogen evolution overpotential is very small, 0.025% PTFE, 0.025% Dy<sub>2</sub>O<sub>3</sub> and their combined additive increase the polarization potential of hydrogen evolution, but they can accelerate the hydrogen evolution when the negative plate contains AC, EG or FG with low impurity content or their overpotential of hydrogen



evolution is very high. In the charge of VRLA batteries, the cathodic polarization of the negative plates is very small because of the depolarization of oxygen cycle. It implies that PTFE and Dy<sub>2</sub>O<sub>3</sub> additives can suppress the hydrogen evolution effectively.

Although the acetylene black has very low impurity content and high overpotential of hydrogen evolution, PTFE, Dy<sub>2</sub>O<sub>3</sub> additives and their combined additive can still increase the polarization potential of hydrogen evolution, which is different from what happens in the case of AC, EG and FG materials. And the combined additives of PTFE and Dy<sub>2</sub>O<sub>3</sub> greatly increase the charge efficiency of the 12 V 12 Ah VRLA battery with the negative plate containing acetylene black and thus decreases water loss in the test of cycle life.

#### ACKNOWLEDGEMENTS

The authors thank for the financial support of this work by the Natural Science Foundation of Fujian Province (No. 2013J01039).

#### References

1. R. Wagner, *J. Power Sources*, 144 (2005) 494–504.
2. M. Chen, W. Guo, M. Zhang, F. Cheng, P. Liu, Z. Cai, Y. Zhang, *Electrochim. Acta*, 164 (2015) 243–251.
3. J. Xiang, P. Ding, H. Zhang, X. Wu, J. Chen, Y. Yang, *J. Power Source*, 241 (2013) 150–158.
4. L.T. Lam, N.P. Haigh, C.G. Phyland, A.J. Urban, *J. Power Sources*, 133 (2004) 126–134.
5. P. Bača, P. Křivík, J. Zimáková, D. Fryda, *Int. J. Electrochem. Sci.*, 10 (2015) 10307–10320.
6. M. Saravanan, M. Ganesan, S. Ambalavanan, *J. Electrochem. Soc.*, 159 (2012) A452–A458.
7. J. Furukawa, T. Takada, D. Monma, L.T. Lam, *J. Power Sources*, 195 (2010) 1241–1245.
8. P.T. Moseley, D.A.J. Rand, *J. Power Sources*, 133 (2004) 104–109.
9. G.J. May, *J. Power Sources*, 133 (2004) 110–115.
10. L.T. Lam, R. Louey, N.P. Haigh, O.V. Lim, D.G. Vella, C.G. Phyland, L.H. Vu, J. Furukawa, T. Takada, D. Monma, T. Kano, *J. Power Sources*, 174 (2007) 16–29.
11. D. Pavlov, P. Nikolov, *J. Electrochem. Soc.*, 159 (2012) A1215–A1225.
12. A. Cooper, J. Furakawa, L.T. Lam, M. Kellaway, *J. Power Sources*, 188 (2009) 642–649.
13. A.G. Pandolfo, A.F. Hollenkamp, *J. Power Sources*, 157 (2006) 11–27.
14. L.T. Lam, R. Louey, *J. Power Sources*, 158 (2006) 1140–1148.
15. K. Nakamura, M. Shiomi, K. Takahashi, M. Tsubota, *J. Power Sources*, 59 (1996) 153–157.
16. M. Shiomi, T. Funato, K. Nakamura, K. Takahashi, M. Tsubota, *J. Power Sources*, 64 (1997) 147–152.
17. S. Logeshkumar, R. Manoharan, *Electrochim. Acta*, 144 (2014) 147–153.
18. D. Pavlov, P. Nikolov, T. Rogachev, *J. Power Sources*, 196 (2011) 5155–5167.
19. P.T. Moseley, R.F. Nelson, A.F. Hollenkamp, *J. Power Sources*, 157 (2006) 3–10.
20. P.T. Moseley, *J. Power Sources*, 191 (2009) 134–138.
21. J. Valenciano, A. Sánchez, F. Trinidad, A.F. Hollenkamp, *J. Power Sources*, 158 (2006) 851–863.
22. M. Fernández, J. Valenciano, F. Trinidad, N. Muñoz, *J. Power Sources*, 195 (2010) 4458–4469.
23. S.W. Swogger, P. Everill, D.P. Dubey N. Sugumaran, *J. Power Sources*, 261 (2014) 55–63.
24. K. Yang, L. Peng, D. Shu, C. Lv, C. He L. Long, *J. Power Sources*, 239 (2013) 553–560.
25. M. Saravanan, M. Ganesan, S. Ambalavanan, *J. Power Sources*, 251 (2014) 20–29.
26. X. Zou, Z. Kang, D. Shu, Y. Liao, Y. Gong, C. He, J. Hao, Y. Zhong, *Electrochim. Acta*, 151 (2015) 89–98.
27. D. Pavlov, T. Rogachev, P. Nikolov, G. Petkova, *J. Power Sources*, 191 (2009) 58–75.

28. K.R. Bullock, *J. Power Sources*, 195 (2010) 4513–4519.
29. D. Berndt, *J. Power Sources*, 154 (2006) 509–517.
30. K.C. Leonard, A.J. Bard, *J. Am. Chem. Soc.*, 135 (2013) 15885–15889.
31. L.T. Lam, H. Ceylan, N.P. Haigh, T. Lwin, D.A.J. Rand. *J. Power Sources*, 195 (2010) 4494–4512.
32. Y. Wu, W. Li, X. Long, F. Wu, H. Chen, J. Yan, C. Zhang, *J. Power Sources*, 144 (2005) 338–345.
33. W. Li, H. Chen, X. Long, F. Wu, Y. Wu, J. Yan, C. Zhang, *J. Power Sources*, 158 (2006) 902–907.
34. L.T. Lam, J.D. Douglas, R. Pillig, D.A.J. Rand, *J. Power Sources*, 48 (1994) 219–232.
35. Y. -D Cho, G.T. -K Fey, *J. Power Sources*, 184 (2008) 610–616.
36. D. Berndt, *J. Power Sources*, 95 (2001) 2–12.
37. D. Pavlov, A. Kirchev, B. Monahov, *J. Power Source*, 144 (2005) 521–527.
38. A. Kirchev, D. Pavlov, *J. Power Sources*, 162 (2006) 864–869.
39. H. Li, H. Liu, Q. Wang, H. Chen, A. Ren, J. Hu, *Electrochim. Acta*, 56 (2010) 663–666.
40. G. Petkova, P. Nikolov, D. Pavlov, *J. Power Sources*, 158 (2006) 841–845.
41. K. Sawai, T. Funato, M. Watanabe, H. Wada, K. Nakamura, M. Shiomi, S. Osumi, *J. Power Sources*, 158 (2006) 1084–1090.
42. N. Hirai, T. Tanaka, S. Kubo, T. Ikeda, K. Magara, I. Ban, M. Shiota, *J. Power Sources*, 158 (2006) 1106–1109.
43. D. Pavlov, P. Nikolov, T. Rogachev, *J. Power Sources*, 195 (2010) 4435–4443.
44. L. Zhao, B. Chen, J. Wu, D. Wang, *J. Power Sources*, 248 (2014) 1–5.

© 2016 The Authors. Published by ESG ([www.electrochemsci.org](http://www.electrochemsci.org)). This article is an open access article distributed under the terms and conditions of the Creative Commons Attribution license (<http://creativecommons.org/licenses/by/4.0/>).